




# Influence of typical elements and heat treatment parameters on hardenability in steel: a review

Bin-bin Wang<sup>1</sup> · De-xin Zhu<sup>1</sup> · Chao-lei Zhang<sup>1,2</sup> · Xiao-ye Zhou<sup>3</sup> · Hong-hui Wu<sup>1,2,4</sup>  · Shui-ze Wang<sup>1,2</sup> · Gui-lin Wu<sup>1,2</sup> · Jun-heng Gao<sup>1,2</sup> · Hai-tao Zhao<sup>1,2</sup> · Xin-ping Mao<sup>1,2</sup>

Received: 5 May 2024 / Revised: 18 June 2024 / Accepted: 26 June 2024  
© China Iron and Steel Research Institute Group Co., Ltd. 2024

## Abstract

The hardenability of steel is crucial for its durability and performance in engineering applications, significantly influencing mechanical properties such as hardness, strength, and wear resistance. As the engineering field continuously demands higher-performance steel materials, a deep understanding of the key influencing factors on hardenability is crucial for developing quality steel that meets stringent application requirements. The effects of some specific elements, including carbon (C), vanadium (V), molybdenum (Mo), and boron (B), as well as heat treatment process parameters such as austenitizing temperature, austenitizing holding time, and cooling rate, were examined. It aims to elucidate the interactions among these factors and their influence on steel hardenability. For each influencing factor, the heat treatment procedure, characteristic microstructure resulting from it, and corresponding Jominy end quench curves were discussed. Furthermore, based on the continuous development of big data technology in the field of materials, the use of machine learning to predict the hardenability of steel and guide the design of steel material was also introduced.

**Keywords** Hardenability · Jominy end quench test · Heat treatment · Steel hardness · Austenite · Martensite

## 1 Introduction

In steel machinery manufacturing, hardenability is a crucial criterion for selecting the appropriate steel type for part fabrication and determining the heat treatment process during production [1–10]. Hardenability, distinct from hardening capacity, denotes the depth to which steel can be hardened through quenching [11]. This indicates that high

surface hardness in steel does not ensure uniform hardness throughout its interior. Conversely, steel with lower surface hardness can achieve consistent hardening from surface to core, demonstrating the quenching capability of steel. The assessment and comprehension of steel hardenability hold significant practical relevance. For instance, selecting steel grades with lower hardenability may be more economical for workpieces where internal mechanical properties minimally affect their operational conditions. However, for workpieces requiring uniform mechanical properties throughout their entire cross-section, selecting a steel grade that ensures adequate hardenability is crucial [12]. In scenarios where sufficient hardenability is ensured, using milder quenching media during heat treatment is preferable, as it helps to reduce stress and deformation of the workpiece during processing [13, 14]. For workpieces with large cross-sections, only steel grades with suitably high hardenability can ensure the desired hardenability, thereby ensuring uniform microstructure and mechanical properties. Furthermore, for mechanical components subjected to heavy loads, selecting steel grades with optimal hardenability is essential for achieving superior mechanical properties. Therefore, the selection of appropriate types of

---

Bin-bin Wang and De-xin Zhu have equally contributed to this work.

✉ Chao-lei Zhang  
zhangchaolei@ustb.edu.cn

✉ Hong-hui Wu  
wuhonghui@ustb.edu.cn

- <sup>1</sup> Institute for Carbon Neutrality, University of Science and Technology Beijing, Beijing 100083, China
- <sup>2</sup> Institute of Steel Sustainable Technology, Liaoning Academy of Materials, Shenyang 110004, Liaoning, China
- <sup>3</sup> Department of Materials Science and Engineering, Shenzhen MSU-BIT University, Shenzhen 518172, Guangdong, China
- <sup>4</sup> Institute of Materials Intelligent Technology, Liaoning Academy of Materials, Shenyang 110004, Liaoning, China

steel based on their hardenability is a key consideration in applications [15].

The hardenability of different steel types varies substantially, mainly influenced by chemical composition, heat treatment processes, and microstructure [16–24]. Chemically, steel primarily consists of iron (Fe), carbon (C), and various alloying elements. When dissolved in austenite, most of these elements, except cobalt (Co), shift the isothermal transformation curve of austenite to the right. This shift increases the stability of austenite, thereby enhancing the hardenability of steels by reducing the critical cooling rate. To examine the effect of boron (B) on hardenability in boron steel, Hwang et al. [25] conducted hardenability tests on standard boron steel, molybdenum (Mo)-containing boron steel, and chromium (Cr)-containing boron steel at various austenitizing temperatures. It was found that solute B, when it accumulates at the boundaries of austenite grains, significantly delays the initiation of pro-eutectoid ferrite at these boundaries by reducing the interface energy between neighboring austenite grains, thus enhancing hardenability. To investigate the effect of vanadium (V) on the hardenability of 40CrNiMoV steel, Chen et al. [26] performed Jominy end quench tests. It was observed that aluminum (Al) effectively stabilizes nitrogen, and this process facilitates the solid solution distribution of V along grain boundaries, delays the transformation to ferrite, and increases the stability of austenite, potentially improving the steel hardenability. Despite extensive research into the effects of various chemical compositions on steel hardenability, a systematic summary of this aspect is lacking.

The heat treatment process is another pivotal factor influencing the hardenability of steel, particularly through changes in grain size and the distribution of alloying elements within the microstructure. To study the influence of austenitization temperature and cooling rate on the hardness distribution, Nunura et al. [27] conducted Jominy end quench experiments on AISI 1045 steel. The results indicate that the microstructure morphology varies with austenitizing temperature, with a corresponding increase in hardness observed after end quench. To assess the effect of austenitizing degree on the hardenability of ductile iron, Fernandino et al. [28] performed Jominy end quench tests on ductile iron subjected to varying austenitization levels. The result indicates that at lower austenitization temperatures, the hardenability of incompletely austenitized samples was significantly reduced compared to that of fully austenitized samples. Although many studies that have explored the influence of austenitizing temperature, holding time, and cooling rate on steel hardenability, a comprehensive overview of the effect of the heat treatment process on hardenability is still lacking.

In the present work, the influences of some key alloying elements, heat treatment parameters, and other factors on

steel hardenability are summarized. For each influencing factor, this article describes the heat treatment procedure, microstructure, and hardness testing. In addition, development trends in hardenability are also discussed in the review. This article aims to guide the application of hardenability in the development and production of steel and deepen the influence of hardenability in the field of materials science.

## 2 Influence of alloying elements and heat treatment on hardenability

To further explore the factors influencing hardenability, it is imperative to examine the factors affecting the hardenability. The critical cooling rate of steel, defined as the minimum rate of cooling that results exclusively in martensitic transformation during quenching, serves as a vital benchmark for assessing steel hardenability. The elemental composition of steel and its pre-quenching heat treatment history significantly affect this critical cooling rate, and the cooling rate during quenching determines the complete realization of the hardenability [29]. Typically, the thermal expansion method is employed to construct the continuous cooling transformation (CCT) curve to measure the critical cooling rate of steel, which reflects its hardenability [30–33]. In addition, the Jominy end quench test is frequently utilized to generate the end quench curve, providing a representation of the hardenability in steel [27, 34–38]. The end quenching experiment is a well-defined procedure for assessing the hardenability of steel. Initially, the specimen is normalized and shaped into a standard size of 25 mm in diameter and 100 mm in length. After quenching, opposite sides of the entire length of the sample are ground down to a specified depth to create two parallel planes, and subsequently, measurements of the Rockwell hardness (HRC, and in certain instances, Vickers hardness or Brinell hardness) begin with the water-cooled end along the centerline of the ground plane, at predefined intervals. As the hardness values decrease and stabilize, the intervals for measuring hardness can be expanded, continuing until the required distance from the water-cooled end is reached [39–41]. This review primarily discusses the aforementioned experimental techniques to measure the hardenability of steel. The addition of alloying elements significantly improves the hardenability of steel. For instance, C is fundamental element in steels, and the hardenability increases as the C content rises to eutectoid point, whereas it decreases when the C content further increases beyond eutectoid point. C serves as a primary hardener in steel, and its presence is crucial for determining the steel hardenability. Besides, the effect of V on hardenability is complex, depending on its existing state. V

improves the hardenability of steel in the solid solution state but reduces it when presenting as a compound [26]. In addition, adding a minor amount of B (0.001–0.003 wt.%) markedly enhances hardenability with reduced production costs [42], and adding Mo can further improve the hardenability of B steel (Mo–B combined effect). Therefore, this work selects these four alloying elements as representatives to discuss the effect of alloying elements on hardenability. As shown in Fig. 1, the hardenability of steel can be altered through changes in its composition and processing. Moving forward, the following section delves into the latest research developments regarding the influence of these factors on hardenability.

## 2.1 Influence of C on hardenability

The content of C significantly influences the hardenability of steel [43, 44]. In hypoeutectoid steels, an increase in C content decreases the temperature at which austenite transforms into ferrite and cementite, thereby reducing the required phase transformation driving force. It consequently lowers the critical cooling temperature, enhancing the hardenability of steel. Conversely, in hypereutectoid steels, increasing C content raises the transformation temperature and the necessary driving force for phase transformation, thereby resulting in a higher critical cooling temperature and decreased hardenability [45].

To investigate the effect of C content on the surface hardenability of Cr–Si–Mn low-alloy steel, Wang et al. [46] examined the microevolution and surface hardness changes of Cr–Si–Mn low-alloy steel with different carbon contents after quenching. It was found that with rising C levels, the microstructure of steel progressively shifts from lath martensite to acicular martensite. This transformation,

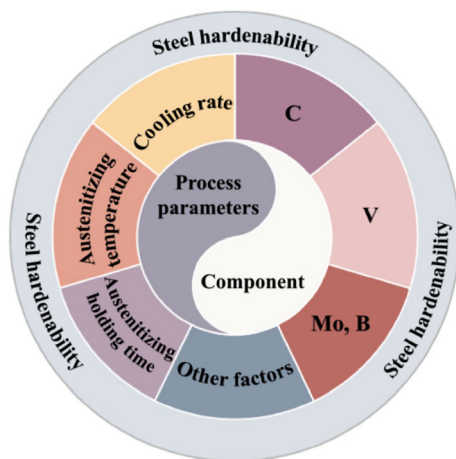


**Fig. 1** Typical factors influencing steel hardenability: components (C, V, Mo, B) and heat treatment parameters (austenitizing temperature, holding time, cooling rate)

alongside increased C supersaturation and martensite refinement, contributes to enhanced hardness. The experimental procedure involved normalizing the ingot at 890 °C for 1 h, followed by austenitization at the same temperature for an additional hour, and subsequent oil quenching. Tempering was carried out at 300 °C for 2 h before air cooling. To mitigate the potential adverse effects of casting defects on the results, specimens for testing were sourced from a specific area located 3 mm below the surface, as illustrated in Fig. 2a. Following heat treatment, the ingots were machined to their final dimensions in compliance with ASTM E23-02 standards. The microstructure of the

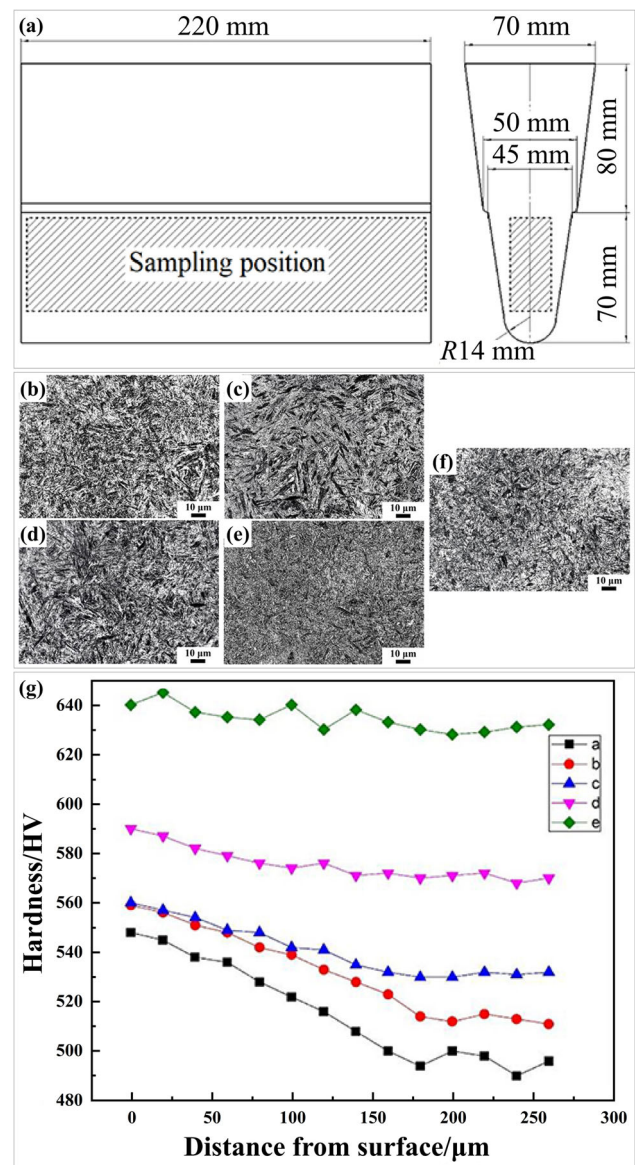


**Fig. 2** Influence of C content on hardenability of Cr–Si–Mn low-alloy steel. **a** Ingot casting and sampling process; **b–f** microstructures of heat-treated specimens at different C concentrations of 0.32, 0.35, 0.40, 0.46 and 0.55 wt.%, respectively; **g** subsurface microhardness distribution across steel samples [46]

specimens with varying C contents is presented in Fig. 2b–f, where it is observed that the metallographic structure is predominantly tempered martensite, exhibiting slight variations in geometric morphology with changes in C content. Specifically, at 0.32 wt.% C, the microstructure is mainly composed of lath martensite, as shown in Fig. 2b. With an increase in C content to 0.35 wt.%, the appearance of acicular martensite becomes noticeable, as displayed in Fig. 2c. As C content further increases, a gradual reduction in both the size and quantity of lath martensite is observed, as depicted in Fig. 2d–f, with the steel at a C content of 0.46 wt.% demonstrating the most significant refinement in the martensitic lath structure, as highlighted in Fig. 2e. The microhardness testing of steel samples with different C contents, shown in Fig. 2g, indicates a positive correlation between increased C content and enhanced surface hardness of the steel. In addition, Huang et al. [47] investigated the influence of C content on the hardenability of two high-strength low-alloy steels through crystallographic analysis, and their results confirmed the previously discussed findings.

## 2.2 Influence of V on hardenability

The addition of V can enhance hardenability, with the effect depending on whether V is used as an alloying element or a microalloy additive [48–50]. The works conducted by Mangonon [51, 52] and Lagneborg et al. [53] have demonstrated a correlation between V presence and increased hardenability, indicating that V-containing steel exhibits 1.5 times the hardenability of steel without V. However, different results have emerged from other research, challenging the assertion that V universally enhances hardenability. For instance, Garbarz and Pickering [54, 55] found that the nucleation and growth rates of ferrite at grain boundaries are only impeded when microalloying elements like V are present on austenite grain boundaries as solid solutions, not when they form compounds. Thus, the form in which V exists within the microstructure critically influences its effect on hardenability. V easily forms carbonitrides with C and N, such as VC and VN. VC is usually completely soluble at 800–950 °C, while VN is completely soluble above 1000 °C. At high temperatures, the main precipitate in austenite is VN. Generally, by adding elements with high affinity to N (such as Al), the formation of VN is suppressed, and V may exist in a solid solution [26].

To assess the influence of V on the hardenability of round-link chain steel 23MnNiMoCr54, Zhu et al. [30] examined the microstructure and end-quenching hardness distribution of 23MnNiMoCr54 steel and 23MnNiMoCr54V steel by employing the expansion method and Jominy end quench test. Scanning electron microscopy

(SEM), and transmission electron microscopy (TEM) were utilized to characterize the microstructure of steel and the distribution of V atoms. After adding 0.073 wt.% V to 23MnNiMoCr54 steel, it is observed that V delays ferrite transformation and enhances austenite stability by segregating at grain boundaries. This process improves the hardenability of steel and yields superior properties with slow cooling rates. Figure 3a shows the CCT curve of 23MnNiMoCr54V steel, determined using the expansion method after austenitizing at 950 °C for 20 min, with the martensite start point ( $M_s$ ) of the steel measured at 432 °C. Figure 3b–g compares the SEM images of standard 23MnNiMoCr54 steel and V-added 23MnNiMoCr54 steel at distances from 5, 25, and 55 mm from the quenched end. At 5 mm, both steels exhibit regular lath martensite due to cooling rates that meet or exceed the critical rate for martensitic transformation (Fig. 3b and e). At 25 mm, despite reduced cooling rates, 23MnNiMoCr54V steel still shows complete martensitic transformation with a broader lath structure (Fig. 3c), whereas 23MnNiMoCr54 steel begins to display the growth of feathery upper bainite from the grain boundaries (Fig. 3f). At 55 mm, where the cooling rate further decreases, 23MnNiMoCr54V steel maintains the expansion of lath martensite (Fig. 3d), in contrast to 23MnNiMoCr54 steel, which shows granular bainite within the ferritic matrix (Fig. 3g). Figure 3h depicts the end quenching results of the two steels after austenitizing at 950 °C for 30 min. The microstructural observations at various points align with the hardness distribution noted in the Jominy test, indicating that 23MnNiMoCr54V steel demonstrates enhanced hardenability compared to 23MnNiMoCr54 steel.

## 2.3 Influence of Mo and B on hardenability

The addition of trace amounts of B significantly improves the hardenability of steel [10, 56–62]. This enhancement is primarily due to the segregation of B at the austenite grain boundaries, which reduces the energy levels of these boundaries. Consequently, the stability of austenite is increased, and the nucleation of ferrite becomes more challenging [63, 64]. Thus, only free B positively contributes to hardenability [65, 66]. Nevertheless, the formation of borides like BN,  $Fe_{23}(C, B)_6$ , or  $Fe_2B$  reduces the hardenability. Adding Mo to B-alloyed steel further enhances hardenability by preventing the formation of  $Fe_{23}(C, B)_6$ , displaying the synergistic effect of the Mo–B combination. The existence of Mo greatly improves the effect of B, collectively influencing the nucleation and growth of ferrite.

To determine the influence of Mo and B on the hardenability of low carbon steel, Ishikawa et al. [67] tested the critical cooling rate of low carbon steel with different Mo

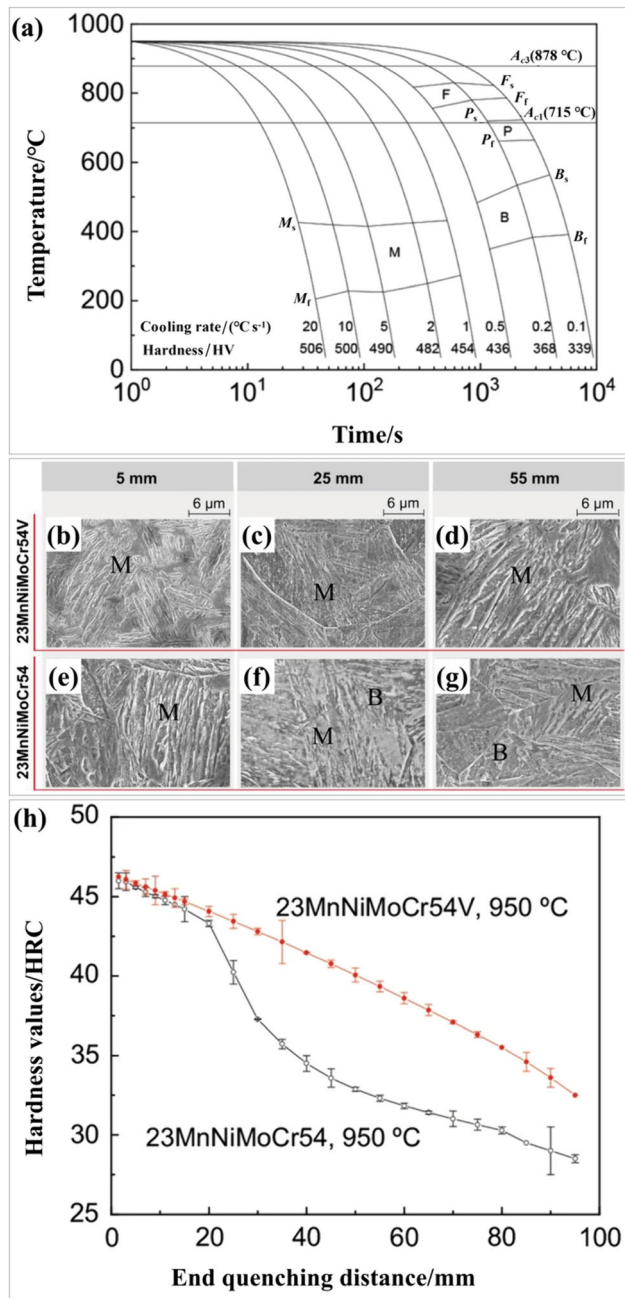


**Fig. 3** Effect of V on hardenability in 23MnNiMoCr54V steel. **a** CCT curve; **b–d** SEM micrographs at various distances from quenched end: V-containing steel at 5, 25, and 55 mm, respectively; **e–g** 23MnNiMoCr54 steel at 5, 25, and 55 mm, respectively; **h** Jominy end quench test profiles for both steels after austenitizing at 950 °C for 30 min [30]. B—Bainite; M—martensite; F—ferrite

and B concentrations. The results showed the addition of trace amounts of boron significantly improves hardenability. Additionally, in B-containing steel, a lower Mo content enhances hardenability, whereas an excess of Mo could diminish it. Figure 4a illustrates the heat treatment process used for samples to study B precipitation. Figure 4b–g

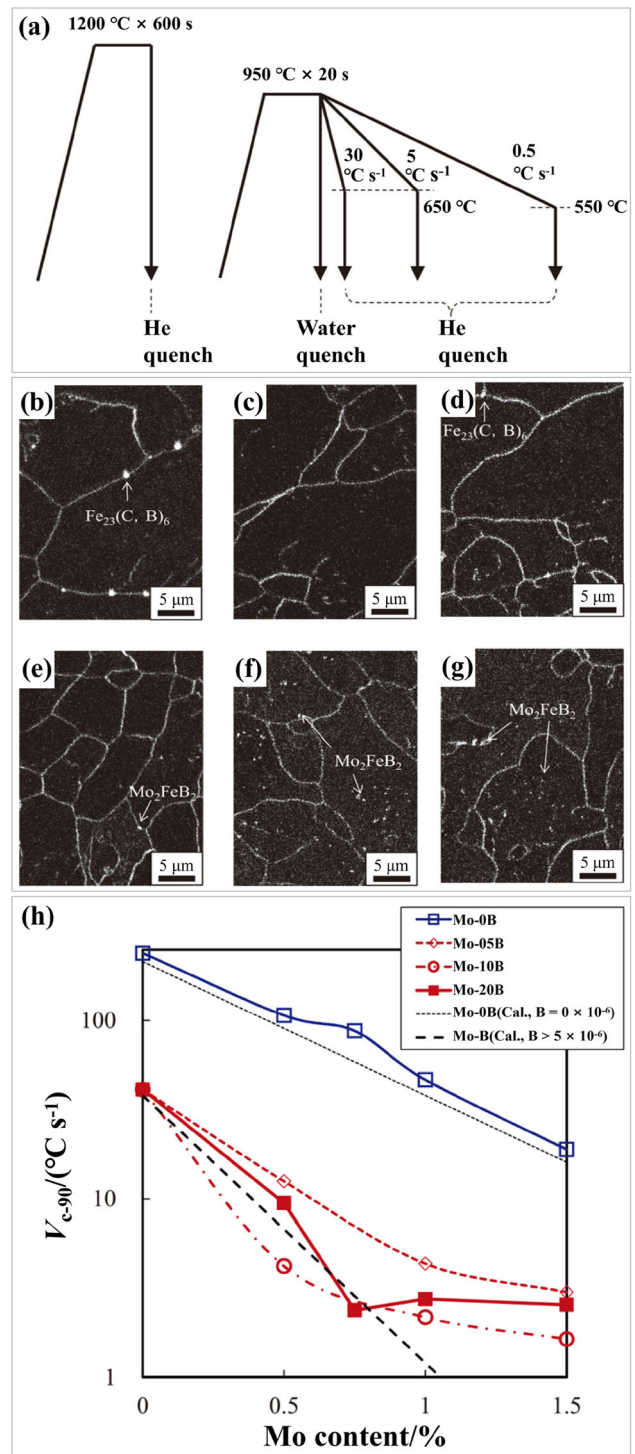


**Fig. 4** Influence of Mo and B on hardenability in low-C boron steel. **a** Thermal patterns analyses from B precipitate samples; **b–g** SIMS images illustrating B-related secondary ion distribution under different thermal conditions: 00Mo10B cooled at 5 °C/s, 05Mo10B cooled at 5 °C/s, 05Mo20B cooled at 5 °C/s, 07Mo20B cooled at 0.5 °C/s, 15Mo20B cooled at 0.5 °C/s, and 15Mo25B immediately water quenched, respectively; **h** effect of Mo content on hardenability ( $V_{c-90}$ ) in steels with and without B [67]

displays secondary ion mass spectrometry (SIMS) results, revealing the distribution of B-related secondary ions under different thermal conditions. Specifically, in Fig. 4b and c, discrete particle signals correspond to  $\text{Fe}_{23}(\text{C}, \text{B})_6$ , whereas continuous line signals denote segregated solute B at former austenite grain boundaries. Notably, in the 15Mo10B steel composition, no B precipitation was detected, even at the slowest cooling rate of 0.5 °C/s. A distinct difference in precipitation behavior between steels with  $20 \times 10^{-6}$  and  $10 \times 10^{-6}$  B content was observed. Specifically, in 05Mo20B steel containing 0.5% Mo,  $\text{Fe}_{23}(\text{C}, \text{B})_6$  precipitation still occurred at former austenite grain boundaries, as illustrated in Fig. 4d. Conversely, no B precipitates were observed in 07Mo20B when cooled at 30 °C/s, indicating that with 0.75% Mo in  $20 \times 10^{-6}$  B steel,  $\text{Fe}_{23}(\text{C}, \text{B})_6$  precipitation can be effectively suppressed during cooling at 30 °C/s. Different boride types, including  $\text{Mo}_2\text{FeB}_2$ , were identified in 07Mo20B and 15Mo20B steel variants at the lowest cooling rate of 0.5 °C/s, with SIMS results presented in Fig. 4e and f. The number of distinct boride particle signals increases with the Mo content. The presence of  $\text{Mo}_2\text{FeB}_2$  phase in the 15Mo25B steel specimen, subjected to water quenching after reheating to 950 °C, suggests its formation during the reheating process, as shown in Fig. 4g. It can be seen from Fig. 4f and g that  $\text{Mo}_2\text{FeB}_2$  exists both at the grain boundaries and within the grains and the effect of  $\text{Mo}_2\text{FeB}_2$  at the grain boundaries on hardenability is dominant. It is because B mainly increases hardenability by segregating to the austenite grain boundaries and inhibiting ferrite nucleation. The formation of borides on the grain boundaries will reduce the B content of grain boundary segregation, thereby reducing the hardenability of the steel [68–70]. Figure 4h explores the influence of Mo content on the critical cooling rate necessary for martensite to constitute 90% ( $V_{c-90}$ ) of the structure post-quench in Mo steel and Mo-B steel. In B-free steel, the  $V_{c-90}$  decreases as Mo content increases. However, in  $20 \times 10^{-6}$  B steel, the  $V_{c-90}$  stabilizes once the Mo content exceeds 0.75%, indicating that at Mo contents above 0.75% in  $20 \times 10^{-6}$  B steel, the beneficial influence of B diminishes, the synergistic Mo–B effect is curtailed, and hardenability starts to decline.

## 2.4 Influence of austenitizing temperature on hardenability

The austenitization temperature significantly influences hardenability [71, 72]. Quenching steels at higher temperatures can improve their hardenability, primarily because elevated temperatures increase the grain size and homogenize the composition, besides facilitating the decomposition of carbides and their dissolution into austenite. Typically, cementite ( $\text{Fe}_3\text{C}$ ) easily decomposes and

dissolves in austenite. However, the presence of elements such as Cr, Mo, and tungsten can lead to the formation of insoluble carbides. For these complex carbides to fully decompose into atoms and diffuse into austenite, a higher austenitization temperature is necessary, which is beneficial for hardenability [73]. Conversely, undissolved carbides can serve as nucleation sites for new phases during phase transformation, accelerating the process, and consequently diminishing hardenability. This also results in an uneven solid solution composition, where areas with lower C and alloy content exhibit increased hardenability. Moreover, higher austenitizing temperatures promote grain growth, further enhancing the hardenability. Nevertheless, excessively high austenitization temperatures may lead to a significant presence of residual austenite post-quenching, and parts will retain more heat. This extends heat transfer to the quenching medium, indirectly reducing cooling rate and thus the hardenability [74].

To explore the influence of austenitizing temperature on the hardenability of martensitic steel X30Cr13, Landgraf et al. [75] performed Jominy end quench tests on X30Cr13 steel treated with different austenitizing temperatures. It was revealed that an increase in austenitizing temperature leads to grain growth and gradual dissolution of carbides, alongside a rise in the amount of alloying elements dissolved in the austenite, thereby enhancing the hardenability of steel. However, upon reaching an austenitizing temperature of 1050 °C and beyond, the quantity of residual austenite after quenching rises incrementally, reducing the overall hardness, and thereby decreasing the hardenability of the steel. Figure 5a presents the time–temperature curve for heat treatment, as recorded by thermocouples, showcasing a good correlation between the experimental and simulation data. Figure 5b–e displays representative optical micrographs of X30Cr13, illustrating changes in carbide content, grain size, and retained austenite in relation to austenitization temperature and the distance from the quenched end face of the bar. Comparing Fig. 5b with d and c with e, it is evident that increasing the austenitization temperature leads to a decrease in the number of carbides, an enlargement of grain size, and an increase in amount of retained austenite. Figure 5f outlines the relationship between hardness distribution, as determined by the end quench experiment, and the distance from the quenching end face in the Jominy end quench test. The results indicate that hardenability improves when the austenitizing temperature increases from 1000 to 1050 °C but begins to decline upon reaching 1100 °C.

## 2.5 Influence of austenitizing holding time on hardenability

As the austenitizing holding time is extended, carbides dissolve more thoroughly, austenitization becomes more

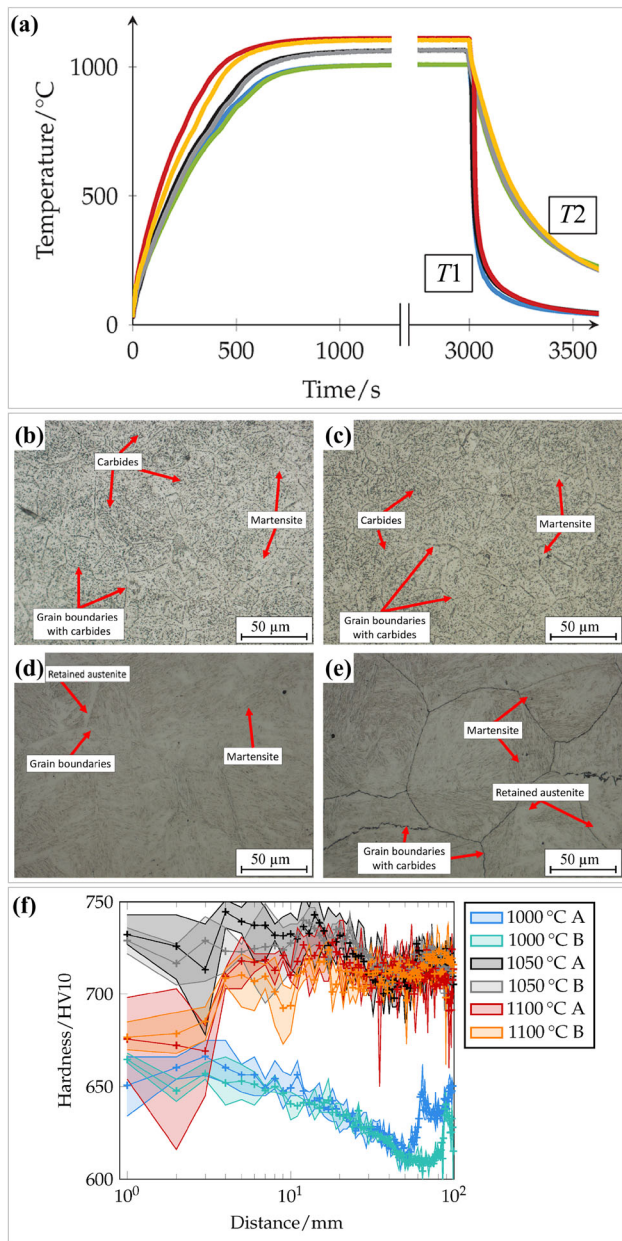


**Fig. 5** Influence of austenitizing temperature on hardenability in X30Cr13 steel. **a** Heat treatment process flow at varying austenitizing temperatures; **b–e** optical micrographs of X30Cr13 at different austenitizing temperatures and distances from the quenching end: 1000 °C at 1 mm, 1000 °C at 50 mm, 1100 °C at 1 mm, and 1100 °C at 50 mm, respectively; **f** comparison of Jominy end quench curves under different austenitizing temperatures [75]

complete, and hardenability increases. However, excessively long holding time can lead to grain coarsening, excessive precipitation of alloying element phases, a decrease in solid solution element content, and consequently, a reduction in hardenability [37]. The work indicates that excessively extending the holding time is

unnecessary, as it does not significantly alter the main phase of the microstructure. Moreover, reducing the holding time can also help reduce costs [76].

To investigate the effect of holding time on 25CrMo quenched and tempered steel, Zheng et al. [77] performed Jominy end quench tests on 25CrMo steel by changing the austenitizing holding time. The results corroborate the aforementioned theory. Figure 6a shows the heat treatment process flow for different austenitization holding time. Figure 6b–d presents TEM results showcasing the microstructure of Jominy samples at different distances from the water spray nozzle. Figure 6b–d details the microstructure evolution from the nozzle proximity to the midsection and the furthest point. As depicted in Fig. 6b, the structure adjacent to the nozzle primarily consists of martensite. In the midsection, as illustrated in Fig. 6c, there is a predominance of granular bainite accompanied by a minor presence of ferrite, with a noticeable reduction in martensite. Figure 6d reveals that at the furthest extent of the sample, there is only a slight presence of martensite, with ferrite and granular bainite becoming the dominant structures. The size of the ferrite grains increases, and the granular bainite appears coarser as the distance from the water spray nozzle grows, indicating a trend towards increasing amounts of granular bainite and ferrite while martensite decreases. Figure 6e–g presents a schematic diagram that illustrates the arrangement of B atoms in B-containing steel subjected to varying holding time. The diagrams show that extended holding time favors the formation of B-containing phases, which in turn diminishes hardenability. Figure 6h displays the Jominy end quench curve across different holding time, demonstrating that hardenability initially increases with the prolongation of holding time. However, once the holding time exceeds 1 h, further increases result in a decrease in hardenability. This finding suggests that an optimal holding time exists to maximize hardenability, beyond which detrimental effects such as excessive grain growth and phase precipitation begin to outweigh the benefits.

## 2.6 Influence of cooling rate on hardenability

While the cooling rate does not inherently affect the hardenability of steel, it significantly influences the final properties of the workpiece [78, 79]. Faster cooling rates lead to decreased volume fractions and lower C concentrations in retained austenite. They also result in smaller sizes of prior austenite grains, reduced final grain size, and diminished lath dimensions. These changes are associated with increased yield and tensile strength. Conversely, a slower cooling rate tends to decrease the proportion of

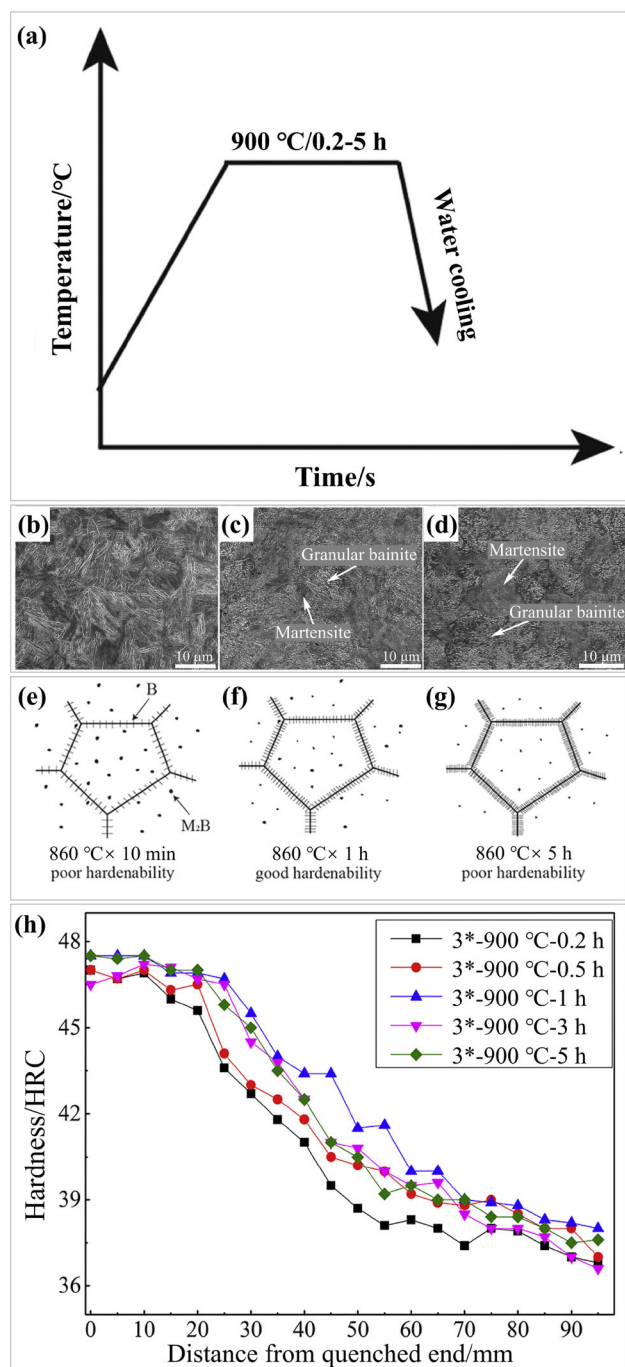


**Fig. 6** Influence of austenitizing holding time on hardenability in 25CrMoNbB steel. **a** Heat treatment process flow for Jominy end quench experiments at varying holding time; **b–d** TEM images at various distances from water spray nozzle: directly at nozzle, 48.5 mm away and 97.0 mm away, respectively; **e–g** schematic representation of B atoms arrangement in B-containing steel at holding time of 10 min, 1 h and 5 h; **h** Jominy end quench curves across different holding time [77]

martensite structure and increase the presence of bainite or other microstructures, thereby reducing the hardness of steel. In addition, the larger grain size associated with

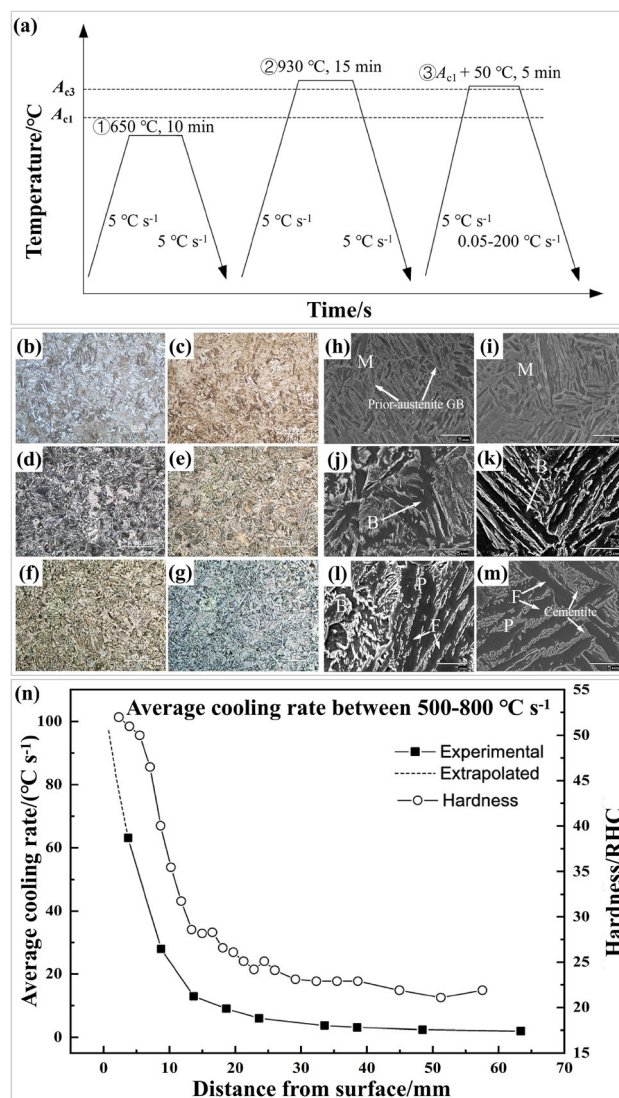


**Fig. 7** Influence of cooling rate on hardenability in S34MnV steel. **a** Heat treatment process flow for CCT samples; **b–m** optical microscopy and SEM images at various distances from quenching end surface: 0 mm (**b, h**), 3 mm (**c, i**), 18 mm (**d, j**), 23 mm (**e, k**), 48 mm (**f, l**), 63 mm (**g, m**); **n** cooling rate and HRC profile as a function of distance from sample end-face [82]

slower cooling rates may adversely affect the toughness of steel [80, 81].

To explore the effect of cooling rate on the hardenability, microstructure, and phase transformation of S34MnV steel, Chen et al. [82] conducted Jominy end quench tests on S34MnV steel and observed its microstructure. They developed a continuous cooling transformation diagram from thermal expansion experiments and analyzed the crucial influence of cooling rate on the final hardness, phase transformation, and microstructure of the steel. The heat treatment process used to produce the CCT curve in the expansion test is shown in Fig. 7a. Figure 7b and c presents the microstructure



observed 3 mm away from the quenching end, characterized predominantly by lath martensite. Figure 7h and i illustrates the respective SEM microstructures. The strip dimensions in the final piece shown in Fig. 7h are greater than those located 3 mm from the quenched end as seen in Fig. 7i. As depicted in Fig. 7h, a single lath forms a block at the prior austenite grain boundary. As the distance from the water quenching end increases, the cooling rate decreases, leading to the formation of new phases. With a reduction in the cooling rate, phases such as upper bainite, pearlite, and ferrite become more apparent, and their occurrence increases with distance from the quenching end, sometimes appearing intermixed, as presented in Fig. 7j–m. In Fig. 7l and m, the microstructure primarily consists of pearlite, characterized by bright gray cementite structures segmented by dark areas or black pro-eutectoid ferrite regions. Figure 7n illustrates that with increasing distance from the quenching end, the cooling rate continues to decline, and correspondingly, the hardness decreases. The comparison between the hardness curve and the cooling rate curve in the figure reveals similar patterns, indicating that the hardness is significantly affected by the cooling rate.

## 2.7 Influence of additional factors on hardenability

The uniformity of austenite significantly affects the critical cooling rate, generally leading to decreased hardenability. When segregation occurs in steel, alloying elements and impurities are concentrated at these sites, reducing the effective components in other areas of the steel. This segregation shifts the position of the isothermal transformation curve upward, increases the critical cooling rate, and causes phase transformation reactions to initiate earlier. Additionally, even though alloying elements in steel may be completely dissolved in austenite, their distribution can remain non-uniform. During phase transformation, the concentration differences accelerate diffusion, which increases the nucleation rate of new phases [83, 84].

The actual grain size of austenite also markedly affects the critical cooling rate value of steel. Proeutectoid and pearlite nuclei generally tend to form primarily at the austenite grain boundaries and then grow into coarse austenite grains. Smaller grain sizes mean increased grain boundaries, offering more sites for the nucleation of pearlite, thus weakening hardenability. Conversely, larger grains extend the incubation period of austenite, reducing the critical quenching speed required for steel. Therefore, incorporating alloying elements that inhibit austenite grain growth in steel can elevate the critical cooling rate, subsequently reducing the hardenability of steel [85–88].

Non-metallic inclusions such as sulfides, nitrides, oxides, and other dispersed particles can inhibit the growth of austenite grains at heating temperatures. During quenching and rapid cooling, their dispersed distribution promotes the formation of crystal nuclei, accelerating the transformation of austenite and consequently reducing hardenability. For example, Ren et al. conducted a novel hybrid heat treatment technique for martensitic steel, resulting in the formation of a hard layer of nitrogen-stabilized austenite [89, 90].

Stable carbides, such as those formed by V, titanium (Ti), and niobium (Nb), are difficult to dissolve into austenite at standard heating temperatures. They hinder grain growth and refine austenite grains, leading to a reduction in the C content of the austenite. Both factors increase the critical cooling rate, thereby reducing the hardenability of steel. However, when these elements are heated at higher temperatures and maintained for sufficient holding time to allow the carbides to dissolve into the solid solution, they can reduce the critical cooling rate, thereby enhancing hardenability [91, 92].

## 3 Discussion

After years of development, the studies on hardenability have achieved lots of progress, yet aligning hardenability with other mechanical properties continues to pose challenges. The preceding sections have thoroughly examined how various components and processes influence steel hardenability. It is important to recognize that these factors often operate in conjunction during the actual steel production process. For instance, in practical steel production, the combination of Mo and B significantly improves hardenability; Nb can markedly enhance steel hardenability at higher austenitizing temperatures; and the level of austenitizing temperature also affects the state of the alloying elements in the microstructure, collectively influencing the hardenability of steel [93].

In the past, experimental statistics often relied on derived empirical formulas, which were constrained by the knowledge and experience of experts [94]. These formulas with complex, nonlinear form and typically required manual updates and adjustments to adapt to new data and situations. In contrast, machine learning models use datasets and algorithms to improve generalization, adaptability, and accuracy. Moreover, they are more effective in uncovering the relationships between alloying elements, process parameters, and hardenability [95].

Recent studies have explored the use of machine learning to predict the hardenability of steel. For instance, Dong et al. [96] conducted a comparative study using various machine learning methods to develop a model that

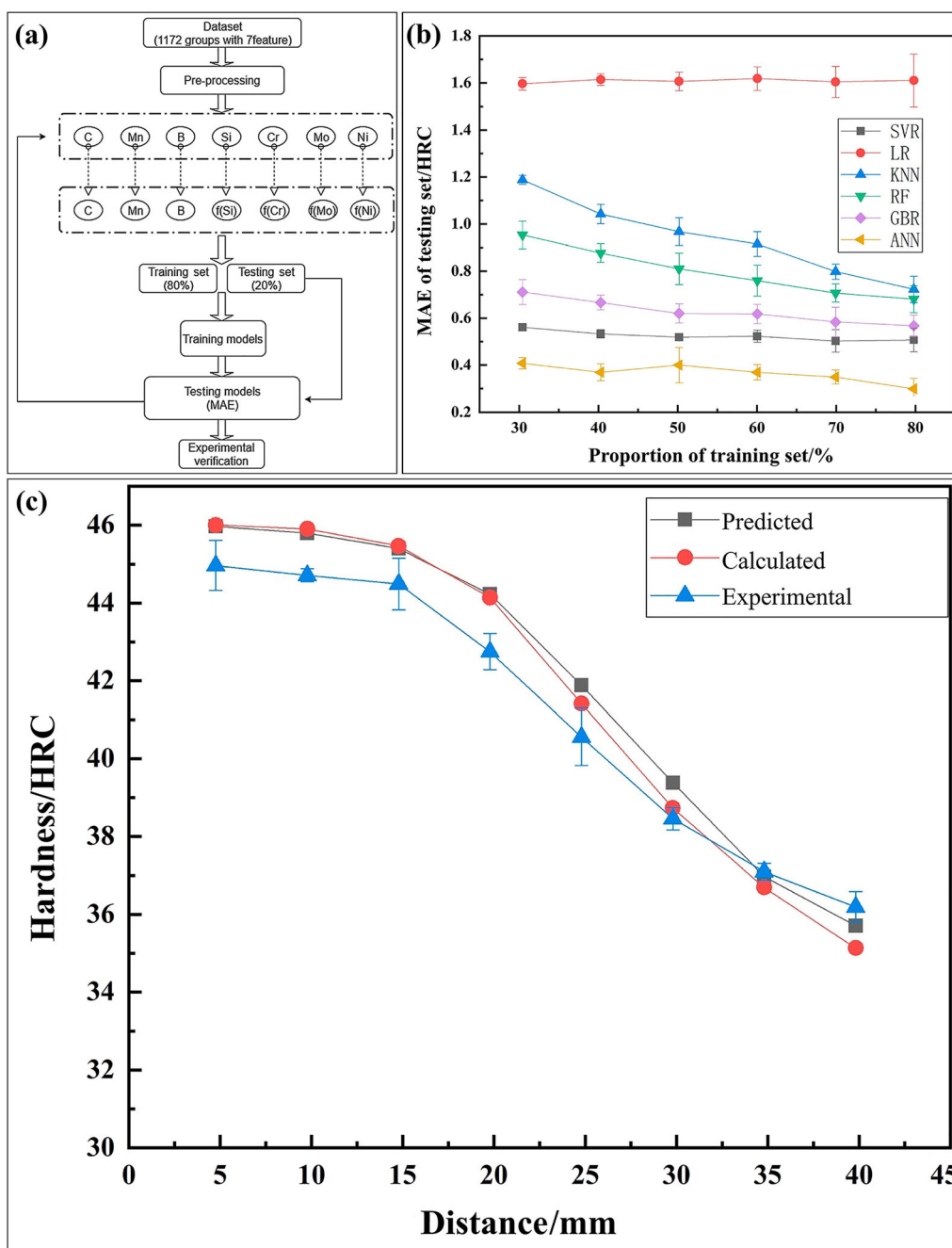


**Fig. 8** Prediction of steel hardenability using machine learning. **a** Process of machine learning for predicting hardenability in wear-resistant steel; **b** MAE values of hardenability models predicted by

different machine learning models; **c** predictive and experimental hardenability curves: ANN predictions, JMatPro calculations, and experimental measurements [96]

correlates the chemical composition of wear-resistant steel with its hardenability. An artificial neural network was employed to perform reverse microalloying design based on targeted performance, offering a practical approach for designing steel compositions. As illustrated in Fig. 8a, the input variables of models include the chemical composition elements C, Si, Mn, Cr, Ni, Mo, and B. The output variables are the relative hardness across different thicknesses.

Figure 8b displays the mean absolute error (MAE) values of different machine learning algorithms for predicting hardenability, highlighting the superior performance of the artificial neural network (ANN) model. Figure 8c compares the predicted values with experimental values, demonstrating the effectiveness of the model. Nenchev et al. [97] developed different machine learning models, ultimately identifying the extreme gradient boosting



can be conducted on steel composition and process parameters to quickly and comprehensively explore the effect of these variables. This method allows for the rapid screening and identification of steel grades with superior hardenability based on their composition and process parameters.

3. Data-driven strategy for steel hardenability: Applying machine learning technologies to existing datasets of steel hardenability can significantly aid the design and development of steel grades tailored to specific requirements. This approach establishes a quantitative correlation between key composition/process parameters and hardenability, thereby facilitating the development of steel designed to meet precise hardenability demands.
4. Integrated computational materials for steel hardenability: Combining computational models with experimental observation can enhance the understanding of how steel microstructure evolution influences hardenability. This integration enables accurate predictions of steel hardenability across different length scales and deepens the understanding of the relationship between microstructural characteristics and hardenability.

By advancing these areas, significant progress can be made in enhancing the development and application of steel with optimized hardenability. These initiatives will not only improve material performance but also contribute to the sustainability and efficiency of steel production processes.

**Acknowledgements** The present work is supported by the National Natural Science Foundation of China (Nos. 52122408 and 52071023). Hong-hui Wu also thanks the financial support from the Fundamental Research Funds for the Central Universities (University of Science and Technology Beijing, Nos. FRF-TP-2021-04C1 and 06500135). The computing work is supported by USTB MatCom of Beijing Advanced Innovation Center for Materials Genome Engineering.

## Declarations

**Conflict of interest** Xin-ping Mao is an editorial board member and Hong-hui Wu is a youth editorial board member for *Journal of Iron and Steel Research International* and they were not involved in the editorial review or the decision to publish this article. The authors declare that they have no known competing financial interests or personal relationships that could have appeared to influence the work reported in this paper.

## References

- [1] M. Maleki, H. Mirzadeh, M. Zamani, *Steel Res. Int.* 89 (2018) 1700412.
- [2] H. Xue, W. Peng, L. Yu, R. Ge, D. Liu, W. Zhang, Y. Wang, *Mater. Sci. Eng. A* 793 (2020) 139901.
- [3] A. Di Schino, P. Emilio Di Nunzio, J. Maria Cabrera, *Adv. Mater. Lett.* 8 (2017) 641–644.
- [4] Y.A. Samoilovich, *Metallurgist* 59 (2015) 604–612.
- [5] G. Balachandran, *IOP Conf. Ser.: Mater. Sci. Eng.* 314 (2018) 012016.
- [6] Y. Zhang, W. Shi, L. Yang, Z. Gu, Z. Li, *J. Mater. Eng. Perform.* 25 (2016) 2727–2735.
- [7] H. Mohrbacher, *Adv. Manuf.* 4 (2016) 105–114.
- [8] L.Y. Pyshmintsev, D.P. Uskov, A.N. Mal'tseva, M.A. Smirnov, Y.N. Goikhenberg, *Metallurgist* 63 (2019) 41–50.
- [9] B. Liščić, B. Smoljan, *Mater. Sci. Forum* 879 (2017) 1807–1812.
- [10] S. de Abreu Martins, C. de Abreu Martins, N. Fonstein, L. Barbosa Godefroid, *Mater. Sci. Forum* 869 (2016) 625–630.
- [11] D.V. Vedybeda, *Metallurgist* 65 (2022) 1054–1061.
- [12] W. Chen, X. Chu, F. Li, J. Liu, H. Lu, S. Kuang, Y. Zou, Z. Zhao, *Steel Res. Int.* 93 (2022) 2200232.
- [13] T. Shrestha, S. Alsagabi, I. Charit, G. Potirniche, M. Glazoff, *Metals* 5 (2015) 131–149.
- [14] J. Grum, *J. Mater. Process. Technol.* 114 (2001) 212–226.
- [15] S. Hu, L. Zhu, M. Zhang, X. Tang, X. Wang, *Materials* 16 (2023) 7413.
- [16] C. Lu, L. Xu, C. Shi, J. Liu, W. Jiang, M. Wang, *Acta Met. Sin.* 56 (2020) 1324–1334.
- [17] E.J. Pavlina, S.J. Lee, E.T. Virtanen, L.M. Rothleutner, C.J. Van Tyne, *Metall. Mater. Trans. A* 42 (2011) 3572–3576.
- [18] B. Hwang, D.W. Suh, *Korean J. Mater. Res.* 23 (2013) 555–561.
- [19] M.V. Maisuradze, M.A. Ryzhkov, *Mater. Sci. Forum* 946 (2019) 341–345.
- [20] Y. Duan, W. Liu, Y. Ma, Q. Cai, W. Zhu, J. Li, *Mater. Sci. Eng. A* 850 (2022) 143599.
- [21] A.I. Potapov, I.T. Malikov, V.I. Urazov, A.E. Semin, *Russ. Metall.* 2010 (2010) 1164–1167.
- [22] S. Ayadi, A. Hadji, *Int. J. Met.* 15 (2021) 510–519.
- [23] M.J. Kim, H.H. Cho, S.H. Kim, S.M. Nam, S.H. Lee, M. Moon, H.N. Han, *Met. Mater. Int.* 19 (2013) 629–635.
- [24] K. Srivatsa, P. Srinivas, G. Balachandran, V. Balasubramanian, *JOM* 68 (2016) 2704–2712.
- [25] B. Hwang, D.W. Suh, S.J. Kim, *Scripta Mater.* 64 (2011) 1118–1120.
- [26] C. Chen, F.C. Zhang, Z.N. Yang, C.L. Zheng, *Mater. Des.* 83 (2015) 422–430.
- [27] C.R.N. Nunura, C.A. dos Santos, J.A. Spim, *Mater. Des.* 76 (2015) 230–243.
- [28] D.O. Fernandez, J.M. Massone, R.E. Boeri, *J. Mater. Process. Technol.* 213 (2013) 1801–1809.
- [29] M. Paczkowska, N. Makuch, M. Kulka, *Opt. Laser Technol.* 102 (2018) 60–67.
- [30] Z. Zhu, Q. Chen, S. Sun, R. Li, J. Qi, H. Liu, Z. Lv, W. Fu, *J. Mater. Eng. Perform.* 30 (2021) 3884–3891.
- [31] B. Hwang, K. Wu, F. Zhou, C. Zhou, M. Zhou, G. Jiao, *J. Mater. Eng.* 2 (2012) 52–55.
- [32] A.B. Rezende, R.S. Miranda, S.T. Fonseca, P.R. Mei, *J. Mater. Eng. Perform.* (2023) <https://doi.org/10.1007/s11665-023-09001-1>.
- [33] G. Pant, A.P. Singh, H.K. Sharma, *Mater. Today Proc.* 26 (2020) 1087–1090.
- [34] N.E. Tenaglia, R.E. Boeri, J.M. Massone, A.D. Basso, *Mater. Sci. Technol.* 34 (2018) 1990–2000.
- [35] M. Çakir, A. Özsoy, *Mater. Des.* 32 (2011) 3099–3105.
- [36] B. Liščić, *Int. Heat. Treat. Surf. Eng.* 8 (2014) 86–92.
- [37] R. Cryderman, T. Ballard, *Metall. Res. Technol.* 115 (2018) 403.
- [38] B. Avishan, M. Abdolalipour Asl Jani, S. Yazdani, *Trans. Indian Inst. Met.* 71 (2018) 493–503.
- [39] J.W. Newkirk, D.S. MacKenzie, *J. Mater. Eng. Perform.* 9 (2000) 408–415.

- [40] D. Hömberg, *Acta Mater.* 44 (1996) 4375–4385.
- [41] M.A. Hassan, M. Mehdi, M. Owais, M. Nasir, S.M.K. Haider, *J. Test. Eval.* 46 (2018) 305–316.
- [42] T. Hara, H. Asahi, R. Uemori, H. Tamehiro, *ISIJ Int.* 44 (2004) 1431–1440.
- [43] İ. Yeğen, M. Usta, *Vacuum* 85 (2010) 390–396.
- [44] A.I.H. Committe, J.L. Dossett, G.E. Totten, *Steel heat treating fundamentals and processes*, ASM International, Materials Park, OH, USA, 2013.
- [45] J. Maity, A. Sharma, *Philos. Mag.* 103 (2023) 407–434.
- [46] X. Wang, Y. Chen, S. Wei, L. Zuo, F. Mao, *Front. Mater.* 6 (2019) 469255.
- [47] S. Huang, B.B. Wu, Z.Q. Wang, Y.S. Yu, C.S. Wang, L. Yan, X.C. Li, C.J. Shang, R.D.K. Misra, *Mater. Lett.* 254 (2019) 412–414.
- [48] H. Adrian, *Mater. Sci. Technol.* 15 (1999) 366–378.
- [49] N. Harada, M. Takuma, M. Tsujikawa, K. Higashi, *Wear* 302 (2013) 1444–1452.
- [50] X. Li, X. Sun, G. Yang, Z. Li, L. Yu, Q. Yong, *J. Mater. Eng.* 1 (2011) 58–62.
- [51] P.L. Mangonon, *Metall. Trans. A* 13 (1982) 319–320.
- [52] P.L. Mangonon, *JOM* 33 (1981) 18–24.
- [53] R. Lagneborg, B. Hutchinson, T. Siwecki, S. Zajac, *The role of vanadium in microalloyed steels*, Swerea KIMAB, Stockholm, Sweden, 2014.
- [54] B. Garbarz, F.B. Pickering, *Mater. Sci. Technol.* 2 (1986) 1016–1114.
- [55] F.B. Pickering, B. Garbarz, *Mater. Sci. Technol.* 5 (1989) 227–237.
- [56] H.R. Lin, G.H. Cheng, *Mater. Sci. Technol.* 3 (1987) 855–859.
- [57] T. Iwamoto, T. Hoshino, A. Matsuzaki, K. Amano, *ISIJ Int.* 42 (2002) S77–S81.
- [58] H. Asahi, *ISIJ Int.* 42 (2002) 1150–1155.
- [59] J.G. Jung, J. Kim, K.M. Noh, K.K. Park, Y.K. Lee, *Sci. Technol. Weld. Join.* 17 (2012) 77–84.
- [60] Y.J. Li, D. Ponge, P. Choi, D. Raabe, *Ultramicroscopy* 159 (2015) 240–247.
- [61] V.S. Kraposhin, A.L. Talis, N.I. Kamenskaya, V. Arestov, A.I. Zaitsev, *Met. Sci. Heat Treat.* 60 (2018) 63–71.
- [62] H.Z. Cui, W.Q. Chen, *J. Iron Steel Res. Int.* 19 (2012) 22–27.
- [63] B. Białobrzeska, *Metals* 11 (2021) 589.
- [64] M. Opiela, *Arch. Mater. Sci. Eng.* 1–2 (2019) 13–23.
- [65] S.P. Ruan, A.M. Zhao, Y.C. Li, M.Y. Guo, Z.Y. Song, *Mater. Sci. Forum* 867 (2016) 24–28.
- [66] F. Beaudet, C. Blais, H. Lehuy, B. Voyzelle, G. L'Espérance, J.P. Masse, M. Krishnadev, *ISIJ Int.* 52 (2012) 424–433.
- [67] K. Ishikawa, H. Nakamura, R. Homma, M. Fujioka, M. Hoshino, *ISIJ Int.* 58 (2018) 551–560.
- [68] S. Watanabe, H. Ohtani, *ISIJ Int.* 23 (1983) 38–42.
- [69] K.A. Taylor, S.S. Hansen, *Metall. Trans. A* 21 (1990) 1697–1708.
- [70] T.S. Prithiv, B. Gault, Y. Li, D. Andersen, N. Valle, S. Eswara, D. Ponge, D. Raabe, *Acta Mater.* 252 (2023) 118947.
- [71] B. Hwang, *Korean J. Mater. Res.* 25 (2015) 497–502.
- [72] A. Kokosza, J. Pacyna, *Mater. Sci. Technol.* 31 (2015) 803–807.
- [73] L.D. Barlow, M. Du Toit, *J. Mater. Eng. Perform.* 21 (2012) 1327–1336.
- [74] A. Rajasekhar, G. Madhusudhan Reddy, T. Mohandas, V.S.R. Murti, *Mater. Des.* 30 (2009) 1612–1624.
- [75] P. Landgraf, P. Birnbaum, E. Meza-García, T. Grund, V. Kräusel, T. Lampke, *Metals* 11 (2021) 1071.
- [76] Z. Li, D. Wu, W. Lü, H. Yu, Z. Shao, L. Luo, J. Wuhan Univ. Technol. *Mater. Sci. Ed.* 30 (2015) 156–161.
- [77] Y. Zheng, F. Wang, C. Li, Y. He, *Mater. Sci. Eng. A* 701 (2017) 45–55.
- [78] T. Korad, M. Polboon, N. Chumchery, J. Pearce, *J. Met. Mater. Miner.* 21 (2011) 67–74.
- [79] A. Grajcar, R. Kuziak, W. Zalecki, *Arch. Civ. Mech. Eng.* 12 (2012) 334–341.
- [80] M. Ali, D. Porter, J. Kömi, M. Eissa, H. El Faramawy, T. Mattar, *J. Iron Steel Res. Int.* 26 (2019) 1350–1365.
- [81] Z.X. Qiao, Y.C. Liu, L.M. Yu, Z.M. Gao, *Appl. Phys. A* 95 (2009) 917–922.
- [82] Z. Chen, P. Nash, Y. Zhang, *Metall. Mater. Trans. B* 50 (2019) 1718–1728.
- [83] D. Li, S. Song, W. Xia, Y. Zhou, Z. Lu, R. Wu, *J. Phys.: Conf. Ser.* 2720 (2024) 012041.
- [84] L. Vilela Costa, D. Corrêa de Oliveira, D. Wallace, V. Lelong, K.O. Findley, *J. Mater. Eng. Perform.* 29 (2020) 3593–3602.
- [85] T. Kasuya, Y. Hashiba, *Shinnittetsu Giho* 385 (2007) 48.
- [86] S. Hanai, N. Takemoto, Y. Tokunaga, Y. Mizuyama, *ISIJ Int.* 24 (1984) 17–23.
- [87] A.D. Schino, *Metalurgija* 56 (2017) 349–352.
- [88] K.Z. Shepelyakovskii, Y.Y. Postnikov, V.D. Kal'ner, L.S. Danil'chenko, *Met. Sci. Heat Treat.* 13 (1971) 713–716.
- [89] N. Ånmark, A. Karasev, P. Jönsson, *Materials* 8 (2015) 751–783.
- [90] Y. Ren, W. Yang, L. Zhang, *ISIJ Int.* 62 (2022) 2159–2171.
- [91] C.I. Garcia, K. Cho, K. Redkin, A.J. Deardo, S. Tan, M. Somani, L.P. Karjalainen, *ISIJ Int.* 51 (2011) 969–974.
- [92] M. Calcagnotto, D. Ponge, D. Raabe, *Metall. Mater. Trans. A* 43 (2012) 37–46.
- [93] R. Esterl, M. Sonnleitner, R. Schnitzer, *Metall. Mater. Trans. A* 50 (2019) 3238–3245.
- [94] J. Trzaska, *Arch. Metall. Mater.* 61 (2016) 1297–1302.
- [95] G. Millner, M. Mücke, L. Romaner, D. Scheiber, *Materialia* 30 (2023) 101810.
- [96] G. Dong, X. Li, J. Zhao, S. Su, R.D.K. Misra, R. Xiao, C. Shang, *Mater. Today Commun.* 24 (2020) 101332.
- [97] B. Nenchev, Q. Tao, Z. Dong, C. Panwisawas, H. Li, B. Tao, H. Dong, *Int. J. Miner. Metall. Mater.* 29 (2022) 836–847.

Springer Nature or its licensor (e.g. a society or other partner) holds exclusive rights to this article under a publishing agreement with the author(s) or other rightsholder(s); author self-archiving of the accepted manuscript version of this article is solely governed by the terms of such publishing agreement and applicable law.